

# Research on Atomic Magnetometers for Magnetocardiography Integrated with Virtual Instrumentation Technology

Xiang Zhao, Xiuyan Ren\*, Kun Xu, Mingxu Zhang, Dan Wu

Department of Nuclear Technology and Application, China Institute of Atomic Energy, Beijing 102413, China.

**Abstract.** This paper presents a new design for an atomic magnetometer for magnetocardiography, which can be easily extended to multi-channel measurements. Virtual instruments are used to demodulate and amplify the photonic signals, enabling signal extraction from input signals with a signal-to-noise ratio of no less than 30 dB. The system based on this design achieves simultaneous demodulation of two-channel signals, with an open-loop sensitivity of  $18 \text{ fT/Hz}^{1/2}$  at 17 Hz and a bandwidth of 128 Hz. In open-loop mode, the system successfully measured an analog magnetocardiogram signal with an amplitude of 100 pT, accurately capturing the P-, QRS-, and T-waveforms, offering a novel approach for multi-channel biomagnetic field measurement.

## 1. Introduction

Weak magnetic field detection plays a significant role in fields such as geophysics, biomedicine, and fundamental physics[1]. Biomagnetic field measurements play a crucial role in non-invasive monitoring of physiological conditions and disease diagnosis, providing essential data [2]. High-sensitivity magnetic detection tools are crucial for achieving these measurements. Unlike conventional superconducting quantum interference devices (SQUIDs), SERF atomic magnetometers deliver enhanced sensitivity, reduced cost, and greater practicality and convenience for biomagnetic field measurements[1, 3].

Most magnetometers obtain magnetic field information through field modulation and lock-in amplification demodulation[4]. Although some use Faraday modulation or photoelastic modulation (PEM) to detect magnetic fields[5], these techniques require dual optical paths, and PEM is bulky, making it difficult to integrate into sensors. In contrast, the single-beam configuration significantly reduces optical path complexity, does not require a Faraday modulator, and is much smaller than the dual-beam setup. Lock-in amplification technology extracts weak signals from large background noise, thereby reducing temperature drift, low-frequency laser noise[6], and environmental common-mode noise in atomic magnetometers[7]. Traditionally, many experimental setups use hardware-based lock-in amplifiers[4, 8]. These hardware lock-in amplifiers, while reliable, are typically single-channel. Adding channels requires additional hardware, increasing system complexity and cost. Demodulated data requires auxiliary outputs or indirect programming extraction, which hinders subsequent data processing.

This work explores the application of virtual instrumentation to atomic magnetometers. The virtual

lock-in amplification function was implemented through LabVIEW programming, enabling accurate extraction of the target signal when the input signal's SNR is no less than 30 dB. This method eliminates the need for multiple hardware lock-in amplifiers, reduces the controller size, and provides greater programming flexibility. Simulated cardiac signal measurements validated the feasibility of this method, which is anticipated to be useful for multi-channel biomagnetic field measurements in the future.

## 2. Principle

Three fundamental components make up a typical atomic magnetometer: an atomic ensemble, a pump laser, and signal detection. The inherent sensitivity of the magnetometer is determined by quantum fluctuations in both the atomic and photon ensembles, with photon shot noise being the limiting factor. The ultimate sensitivity is given by the equation below[9]:

$$\delta B = \frac{1}{\gamma \sqrt{NT_2 V t}} \quad (1)$$

where  $N$  is the atomic density,  $V$  is the volume of the cell,  $t$  represents the measurement time,  $T_2$  is the transverse relaxation time, and  $\gamma$  stands for the gyromagnetic ratio.

However, in practical experiments, the sensitivity is often limited by high-frequency heating and electronic noise in the signal detection devices, and  $\delta B$  is typically expressed as[10]:

$$\delta B = \frac{1}{\gamma} \cdot \frac{\Delta \nu}{\text{SNR}} \quad (2)$$

Here  $\Delta \nu$  corresponds to the linewidth of the magnetic resonance signal (FWHM), and SNR represents the signal-to-noise ratio of the magnetic resonance signal.

\*Corresponding author's e-mail: [rxyl9781974@sina.com](mailto:rxyl9781974@sina.com)

The dynamics of atomic polarization within an ensemble, with the pump laser directed along the z-axis and the external magnetic field applied along the x-axis, are governed by the Bloch equations[2, 10]:

$$\frac{d}{dt} \mathbf{P} = \frac{1}{q(P)} \left[ \gamma_e \mathbf{P} \times \mathbf{B} + R_{op} (\mathbf{s}\hat{z} - \mathbf{P}) - \Gamma \mathbf{P} \right] \quad (3)$$

where  $\gamma_e$  denotes the electron's gyromagnetic ratio,  $q(P)$  describes the electron's deceleration due to hyperfine interactions and spin-exchange collisions, and  $\hat{z}$  indicates the direction of the pump light's propagation. The symbol  $\mathbf{s}$  represents the degree of polarization of the pump light, while  $R_{op}$  refers to the pump rate, and  $\Gamma$  signifies the overall relaxation rate of the atomic ensemble.

The atomic polarization transmission signal, which depends on the magnetic field perpendicular to the laser beam direction, is expressed by the following equation [11]:

$$P_{z-dc}(t) = P_0 \frac{1}{1 + (\gamma B_x \tau)^2} \quad (4)$$

where  $P_0$  represents the effective polarization,  $\tau$  is the spin coherence lifetime.

In magnetometer applications, spin modulation techniques enable operation at low frequencies, thereby reducing the impact of 1/f noise.  $B_x^{mod} = B_1 \cos(\omega_{mod} t)$  is applied along the x-axis.  $\omega_{mod}$  and  $B_1$  represent the frequency and amplitude of the modulated magnetic field, respectively. Alkali-metal atoms experience movement in a magnetic field  $B = (B_x + B_x^{mod}, B_y, B_z)$ , where  $B_x$ ,  $B_y$  and  $B_z$  represent quasi-static magnetic fields. The output signal of the magnetometer system is obtained by nullifying the three-axis magnetic field, as expressed in Equation (3):

$$P_z \propto \text{Re}(P_{\perp}) = S_0 J_0(u) - \gamma_e S_0 J_1(u) B_x \sin(\omega_{mod} t) + 2S_0 J_2(u) \cos(\omega_{mod} t) \quad (5)$$

where  $u = \gamma_e B^{mod} / \omega_{mod}$  represents the modulation parameter,  $P_{\perp}$  refers to the spin polarization, which is oriented perpendicular to the magnetic field,  $S_0 = R_{op} J_0^2(u) / [\Gamma^2 + (\gamma_e B_x)^2]$  is the effective polarization,  $J_n(u)$  represents the Bessel function of the first kind.

For an input reference signal with frequency  $\omega_{mod}$ , the lock-in amplifier generates the amplitude of the demodulated signal after processing the transmitted light, as given by the following equation[12]:

$$V_1 = \frac{\gamma B_x \tau}{1 + (\gamma B_x \tau)^2} \cos(\phi) \quad (6)$$

where  $\phi$  represents the phase difference between the original signal and the reference signal.

### 3. Experimental setup

The experimental setup is depicted in Fig. 1, both as a schematic and as a photograph. At the core of the configuration is an alkali-metal vapor cell, which is filled

with a high concentration of the  $^{87}\text{Rb}$  isotope and contains 600 torr of nitrogen gas to serve as a buffer. The cell has dimensions of  $\phi 3\text{cm} \times 3.2\text{cm}$ . A 300 kHz alternating current is supplied to the heating system, which raises the temperature of the atomic vapor cell to  $150^\circ\text{C}$ . The temperature within the cell is regulated by a non-magnetic pt1000 sensor, maintaining a temperature variation of no more than  $0.01^\circ\text{C}$ . This heating system maintains the high temperatures required for SERF magnetometer operation. The magnetometer is protected by a magnetic shield composed of four  $\mu$ -metal layers and a single layer of aluminum alloy. A commercial fluxgate magnetometer (CH-370) is used to monitor the residual magnetic field, which is less than 3 nT at the center of the shield. Three-axis compensation coils are employed to neutralize both the residual magnetic fields and any virtual fields generated by light frequency shifts. To minimize residual fields and achieve uniform compensation, the vapor cell is placed at the center of the magnetic shield and the compensation coils. The sensitive axes are aligned along the x- and y- directions, with saddle-shaped coils creating magnetic fields that match the shape of the shield. The z-axis coil generates a magnetic field that is aligned with the direction of the pump beam. For accurate magnetic field measurements along the x- and y- axes, two distinct modulation coils are employed to introduce modulated fields in these directions.

An external cavity diode laser (ECDL, DLC pro780, TOPTICA) emits continuous monochromatic light at the  $87\text{Rb}$  D1 line as the pump beam. The Laser Controller and Cosy controller lock the laser frequency. The laser is coupled into a fiber and collimated, resulting in a beam with a diameter of 2.7 mm. The beam then passes through a half-wave plate, followed by a linear polarizer and a quarter-wave plate. The linear polarizer is oriented at a  $45^\circ$  angle with respect to the quarter-wave plate, the linear polarizer converts the linearly polarized light into circularly polarized light, which is then used to pump and polarize the atoms. A photodiode (PD) detects intensity fluctuations caused by polarization, which are then converted into voltage signals by a transimpedance amplifier (TIA, PDA200C, THORLABS). Data acquisition is performed using a PCIe-6374 (National Instruments) card with four channels, featuring a 16-bit ADC and a maximum sampling rate of 3.571 MS/s, enabling simultaneous sampling across all four channels, meeting the sampling requirements and accuracy for virtual lock-in amplification. A virtual lock-in amplifier program was written in LabVIEW, utilizing the PCIe-6374 card. After signal acquisition, the virtual lock-in amplifier demodulates the signal, and real-time magnetic field values are obtained through data processing. A PID control program processes the demodulated signal and uses it to adjust the current supplied to the compensation coils, enabling closed-loop control of the magnetometer. This closed-loop method effectively suppresses magnetic field drift and increases the magnetometer's measurement bandwidth[7, 13]. Locking the magnetic resonance signal at the zero-crossing point enhances the measurement sensitivity to its maximum.

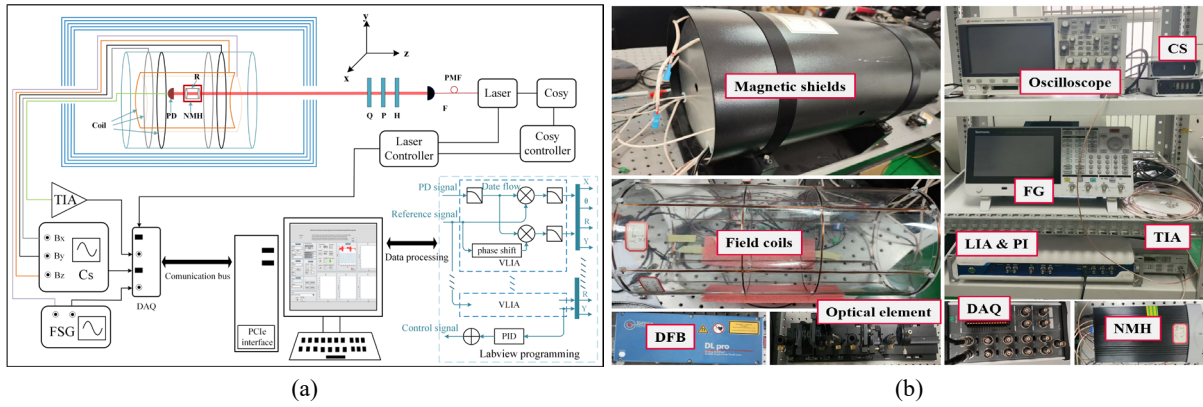


**Fig.1.** (a) Schematic drawing (b) Physical depiction of the experimental system.

## 4. Results and discussion

### 4.1. Demodulation Performance of VLIA and Dual-Channel Demodulation

The virtual lock-in amplifier (VLIA) isolates signal components at the reference frequency while rejecting those at other frequencies. To assess the demodulation performance, sine waves with signal-to-noise ratios (SNRs) of 10 dB, 20 dB, 30 dB, and 40 dB were generated using a signal generator. As illustrated in Fig 2(a), when

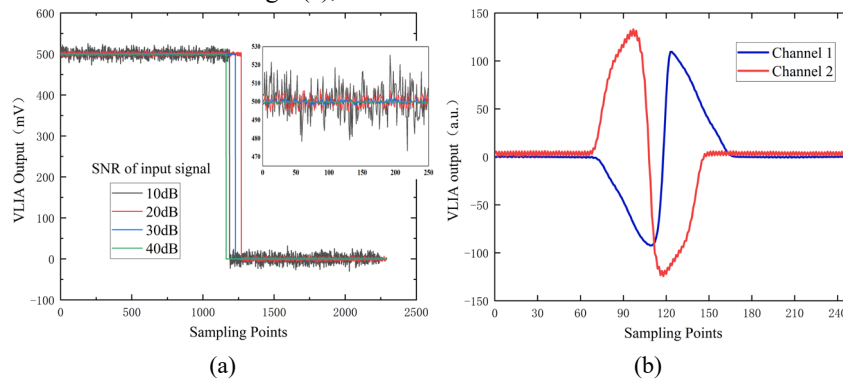


**Fig.2** (a)Response of Virtual Lock-in Amplifier to Signals with Different Signal-to-Noise Ratios. (b)Real-time Dual-Channel Dispersion Curves Collected and Demodulated by VLIA.

### 4.2. Measurement of System Bandwidth and Sensitivity

A sinusoidal magnetic field with an RMS amplitude of 80 pT was applied at various frequencies to assess the magnetometer's response. The VLIA's low-pass filter cutoff was set to 550 Hz, and each measurement of the sinusoidal field lasted 30 seconds, yielding an amplitude-frequency response ranging from 1 Hz to 550 Hz. As shown in Fig. 3(a), the amplitude-frequency response at 1 Hz was used as the reference response. The data across each frequency range were normalized, and the first-order response curve of the low-pass filter was fitted, resulting in a -3 dB bandwidth of 128 Hz. This indicates that the magnetometer system based on virtual lock-in

the input signal frequency matches the reference, higher SNRs lead to improved demodulation performance. The results for 30 dB and 40 dB are nearly identical. When the input signal frequency deviates from the reference, the demodulated signal approaches zero. Fig 2(b) shows the demodulated output from a dual-channel magnetometer utilizing VLIA.

The demodulated signal exhibits a secondary linear shape of the magnetic resonance signal, known as a dispersive line shape. This suggests that virtual lock-in amplification magnetometers are suitable for multi-channel measurements.

amplification meets the frequency range required for magnetocardiogram (MCG) measurements.

To evaluate the sensitivity of the virtual lock-in amplified atomic magnetometer system, the laser frequency was stabilized to the  $^{87}\text{Rb}$  D1 line, the pump light power was set to 4 mW, and magnetic field compensation was applied. The modulation signal frequency and amplitude were adjusted to 1 kHz and 130 nT, respectively. Measurements were performed for 60 seconds in open-loop and closed-loop modes, and the power spectral density was calculated using FFT. In Fig 3(b), the peak at 17 Hz corresponds to the response of the calibrated signal of 80 pTrms. The peaks at 50 Hz and 100 Hz represent power-line noise and its second harmonic, respectively. The magnetometer's open-loop sensitivity in the fig is  $18 \text{ fT/Hz}^{1/2}$ , and the closed-loop sensitivity is  $46 \text{ fT/Hz}^{1/2}$ .

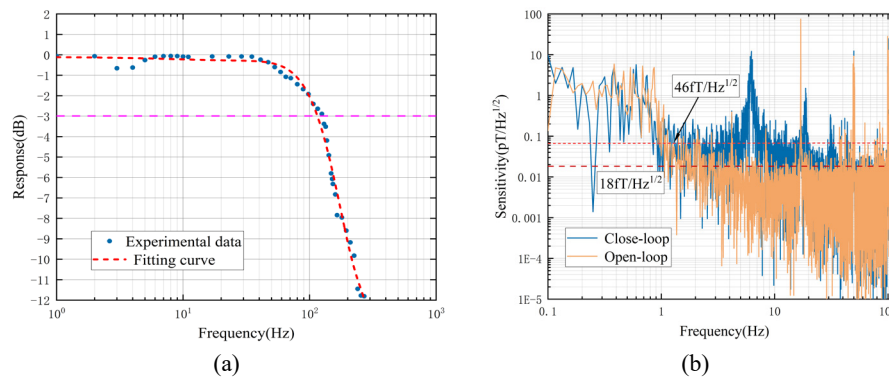


**Fig.3.** (a) The -3dB frequency response of the SERF atomic magnetometer demodulated by VLIA. (b) Power spectral noise in open-loop and closed-loop states, 17 Hz, 80pTrms calibration signal.

### 4.3. Measurement of Simulated Magnetocardiogram (MCG) Signals

To assess the magnetometer system's performance in magnetocardiogram (MCG) measurements, a signal generator created a 2 Hz simulated heart magnetic field along the x-axis with a 100 pTrms amplitude[14]. The modulated signal was transmitted along the x' axis to

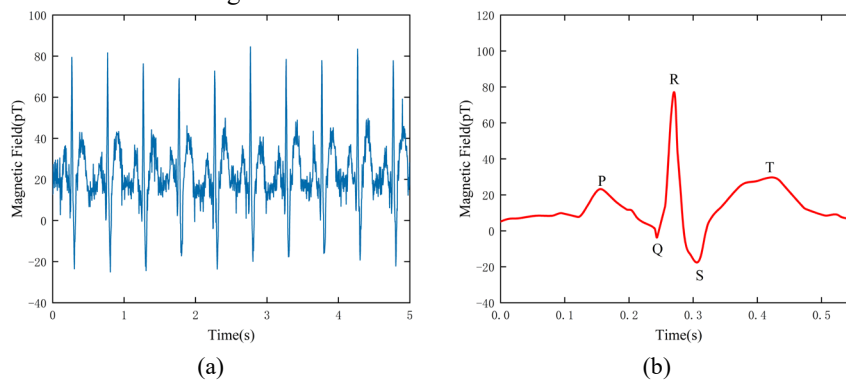


**Fig.4.** (a)The simulated MCG signal recorded by the SERF atomic magnetometer, (b) The filtered data, revealing the complete P-, QRS-, and T-waveforms.

## 5. Conclusion

This study utilizes virtual lock-in amplification technology to demodulate signals in a single-beam atomic magnetometer, reducing the need for hardware lock-in amplifier channels and thereby lowering the cost of multi-channel SERF atomic magnetometers. Experimental results demonstrate that virtual lock-in amplification provides excellent demodulation performance for input signals with a signal-to-noise ratio above 30 dB. The atomic magnetometer system based on virtual instrumentation achieved a bandwidth of 128 Hz and demonstrated a sensitivity of 18 fT/Hz<sup>1/2</sup> at 17 Hz. Finally, the system successfully measured simulated magnetocardiogram (MCG) signals. Future work will focus on the measurement and processing of multi-channel MCG signals.

## Acknowledgments

This work is supported by the China National Nuclear Corporation Young Talents Fund.

ensure optimal demodulation performance. Fig. 4(a) shows the raw heart magnetic field signal measured by the virtual lock-in amplification system. After filtering and smoothing, Fig. 4(b) presents a complete cycle of the heart magnetic signal, including the P-, QRS-, and T-waves. The measurement results indicate that the magnetometer system is capable of accurately capturing the simulated heart magnetic signal, providing an experimental foundation for future multi-channel MCG measurements.

## References

1. M. V. Romalis, J. Wiedemann, S. Zhang, and N. Dural, "Vapor cell Rydberg atom electrometry with time-separated fields," *arXiv preprint arXiv:2406.05106*, 2024.
2. J. Wang, W. Fan, K. Yin, Y. Yan, B. Zhou, and X. Song, "Combined effect of pump-light intensity and modulation field on the performance of optically pumped magnetometers under zero-field parametric modulation," *Physical Review A*, vol. 101, no. 5, pp. 053427, 05/19/, 2020.
3. K. Kamada, Y. Ito, and T. Kobayashi, "Human MCG measurements with a high-sensitivity potassium atomic magnetometer," *Physiological Measurement*, vol. 33, no. 6, pp. 1063-1071, Jun, 2012.
4. L. Li, J. Tang, B. Zhao, L. Cao, B. Zhou, and Y. Zhai, "Single-beam triaxial spin-exchange relaxation-free atomic magnetometer utilizing frequency modulation fields," *Journal of Physics D-Applied Physics*, vol. 55, no. 50, Dec 15, 2022.

5. X. Li, B. Han, K. Zhang, Z. Liu, S. Wang, Y. Yan, and J. Lu, "All-optical dual-axis zero-field atomic magnetometer using light-shift modulation," *Physical Review Applied*, vol. 21, no. 1, pp. 014023, 01/16/, 2024.
6. S. P. Krzyzewski, A. R. Perry, V. Gerginov, and S. Knappe, "Characterization of noise sources in a microfabricated single-beam zero-field optically-pumped magnetometer," *Journal of applied physics*, vol. 126 4, pp. 044504, 2019.
7. J. Tang, Y. Zhai, B. Zhou, B. Han, and G. Liu, "Dual-Axis Closed Loop of a Single-Beam Atomic Magnetometer: Toward High Bandwidth and High Sensitivity," *Ieee Transactions on Instrumentation and Measurement*, vol. 70, 2021, 2021.
8. Z. Ding, J. Yuan, G. Lu, Y. Li, and X. Long, "Three-Axis Atomic Magnetometer Employing Longitudinal Field Modulation," *Ieee Photonics Journal*, vol. 9, no. 5, Oct, 2017.
9. J. C. Allred, R. N. Lyman, T. W. Kornack, and M. V. Romalis, "High-Sensitivity Atomic Magnetometer Unaffected by Spin-Exchange Relaxation," *Physical Review Letters*, vol. 89, no. 13, 2002.
10. M. P. Ledbetter, I. M. Savukov, V. M. Acosta, D. Budker, and M. V. Romalis, "Spin-exchange-relaxation-free magnetometry with Cs vapor," *Physical Review A*, vol. 77, no. 3, 2008.
11. X. Li, Z. Guo, R. Yang, and Y. Feng, "Single-Beam Double-Pass Miniaturized Atomic Magnetometer for Biomagnetic Imaging Systems," *IEEE Sensors Journal*, vol. 23, no. 12, pp. 12433-12440, 2023.
12. Y. Yan, K. Zhang, Z. Liu, Z. Liu, X. Li, Y. Zhou, and J. Lu, "In-situ magnetic fields monitoring and compensation for zero-field atomic magnetometers," *Measurement*, vol. 239, pp. 115410, 2025/01/15/, 2025.
13. W. Lee, *Ultra-High Sensitivity Atomic Magnetometers*, 2022.
14. A.-N. Xu, J. Peng, Y. Yin, and B. Liu, "Single-Beam Atomic Magnetometer Enhanced With Elliptically Polarized Reflected Light," *IEEE Sensors Journal*, pp. 1-1, 2024.